Numerical and Experimental Analysis in Endodontic Rotary Files Under Cyclic Fatigue or Torsional Stress

Damiano Alizzio[a], Fabio Lo Savio[b] and Marco Bonfanti[c]

[a]*Dip. di Ingegneria, Università degli Studi di Messina, C.da Di Dio, 98166 Sant'Agata, Messina,Italy*
[b]*Dip. di Ing. Civile e Architettura, Università di Catania, Catania, CT, Italy*
[c]*Department of Electrical, Electronic and Computer Engineering, University of Catania, Catania, CT, Italy*

Abstract

This study aims to analyze the mechanical behavior of two types of rotating endodontic instruments with different cross sections, both made by Coltene (Hyflex CM 40.04 of NiTi alloy and Hyflex EDM 40.04 of Heat-treated NiTi alloy), under cyclic fatigue or torsion. The study of the mechanical behavior combined the traditional approach, consisting in experimental investigations, with a finite element analysis under similar bending and torque conditions. The non-linear superelastic behavior of the NiTi alloy for fatigue and torsion, derived from experimental tests based on models in the scientific literature, was applied to the numerical analysis. A thermographic investigation was associated with the usual mechanical experimental tests to assess the dependence of the temperature on the deformations undergone by the endodontic files under stress, especially near the breakage. The comparison between experimental and numerical results was in good agreement for both types of files analyzed.

Keywords

Endodontic Instruments, FEA, Cyclic Fatigue, Torsion, Thermography.

1. Introduction

In endodontic therapy, rotary files made of nickel-titanium alloy (NiTi) are widely used when processing the root canal. This is due to the superelasticity and shape memory characteristics of NiTi, which allow it to produce desirable tapered shapes while maintaining flexibility and strength when rotating within curved canals [1]. The shape memory of NiTi alloys derives from a reversible solid-state phase transformation between the austenitic and martensitic structures, known as "thermoplastic martensitic transformation" [2].

Therefore, the NiTi alloy is able to recover its original shape under a range of high deformations. However, NiTi rotary instruments have a high risk of fracture during clinical operation [3]. Many variables might contribute to the file failure, but the two main causes are cyclic fatigue and torsional stress [4, 5, 6, 7, 8]. Cyclic fatigue seems to be more prevalent in curved root canals, whereas torsional failure might occur even in a straight canal [9]. When NiTi rotary instruments are loaded in a cyclic mode, they will undergo both tensile and compressive stress in curved canals. This could cause fatigue failure after a certain number of cycles.

Instead, the torsional failure is characterized by a maximum torsional load and a critical angle of rotation. This reveals the capability of the file to twist before fracture [10].

Differences in cyclic-bending or torsional strength between various NiTi endodontic instruments depend on the different geometries and manufacturing techniques, such as heat treatment, machining, and surface treatments [5, 6, 7, 11, 12].

An alternative to experimental investigations is represented by a numerical method that allows analyzing the mechanical behavior of endodontic files: the Finite Element Analysis (FEA) [13]. FEA calculates stress distributions on files for assigned geometries, material properties and loading conditions, before prototyping [14, 15, 16, 17, 18].

The purpose of this study is to perform a FEA on two types of endodontic files having different cross-section geometries (Hyflex CM 40.04 and Hyflex EDM 40.04 both made by Coltene/Whaledent AG, Altstatten, Switzerland), subjected to bending cyclic fatigue or torsional stress. FEA results will be validated by experimental tests.

2. Materials and Methods

The endodontic instruments object of this study are very different in terms of geometrical and constructive characteristics. EDM 40.04 has a highly variable
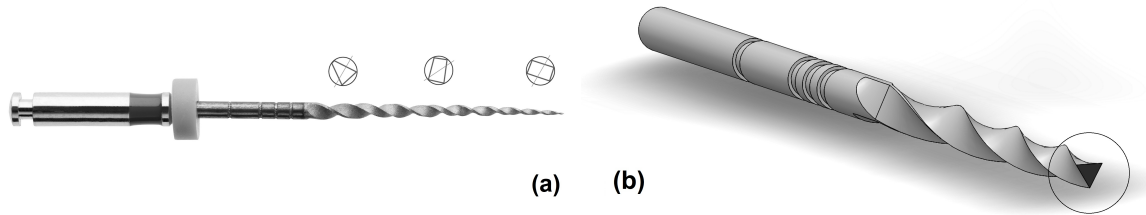
Figure 1: (a) EDM 40.04 and (b) CM 40.04 cross-sections.

Figure 2: Detail of the cyclic fatigue testing device (Courtesy of authors [7]).

Figure 3: Detail of the torsion testing device.

cross-section throughout its length: from a trapezoidal shape (almost triangular) at the beginning of the spiralization, to pseudo-trapezoidal at the central and rectangular close to the tip. Instead, the double-helix model of CM 40.04 determines a triangular cross-section along its entire length, with a decreasing surface as approaching the tip. Figures 1a, 1b show the cross-section of EDM 40.04 and CM 40.04, respectively.

Both types of files were experimentally tested at cyclic fatigue and torsion using two special devices already designed and built by some of the authors [5, 6, 7, 19]. Both apparatuses were designed to assure always the direct view of the rotating file while testing, so to perform a thermal investigation [20, 21]. Then, the methodologies able to detect the thermal variations caused by the crack nucleation and propagation can be successfully used [22].

Figures 2 and 3 show the details of the two measuring devices used for cyclic bending and torsion, respectively.

In the study concerning the cyclic fatigue [6], 80 new Hyflex EDM 40.04 and Hyflex CM 40.04 files of 25-mm length were tested in 2 different groups (at 30° and 60° angles) for each type of file. The curvature radius of the bended file tip was 5 mm; file rotation was set at 300 rpm. The results are summarized in Table 1.

In torsional tests performed in the present study, 40 new Hyflex EDM 40.04 and Hyflex CM 40.04 files were divided in 2 groups. The results are summarized in Table 2. Figures 4a and 5a show the curves relating to the mechanical torsion tests on CM 40.04 and EDM 40.04 files, respectively. Blue and orange curves represent extreme trends of the two sets of #20 files tested. Figures 4b and 5b show an example of the thermal trend of the CM 40.04 and EDM 40.04 files, respectively. In both files, the hotspot corresponds to the spot 2, placed in post-processing near the breakage cross-section, while the spot 6, placed on the stem, maintains a temperature close to ambient temperature.

All data recorded during the cyclic fatigue and torsion tests were statistically analyzed using 2-way analyses of variance (ANOVA) and the Tukey multiple comparison post-hoc test (Prism 7.0; GraphPad Software, Inc., La Jolla, CA) with the significance level established at 5% ($P < 0.05$).

Table 1

Cyclic fatigue test results: mean ± SD of static bending force; number of rotations, dynamic bending and temperature of the hotspot in middle of curvature at breakage. Courtesy of the authors [7].

Instrument	Angle of curvature	Static bending force	No. of rotations at breakage	Dynamic bending force at breakage	Temperature of hotspot at breakage
	[deg]	[N]	-	[N]	[^{o}C]
EDM 40.04	30	0.112 ± 0.030^{a}	2225 ± 176^{a}	1.158 ± 0.045^{a}	33.7 ± 1.4^{a}
	60	0.267 ± 0.011^{b}	1840 ± 163^{b}	1.384 ± 0.051^{b}	36.8 ± 1.6^{b}
CM 40.04	30	0.095 ± 0.018^{a}	$1930 \pm 152^{a,b}$	$1.245 \pm 0.042^{a,b}$	38.2 ± 1.7^{a}
	60	0.728 ± 0.029^{c}	1490 ± 155^{c}	1.512 ± 0.062^{c}	44.6 ± 1.9^{b}
	Different superscript letters in the same column show statistically significant difference ($P > 0.05$)				

Table 2

Torsional test results: mean ± SD of static bending force; number of rotations, dynamic bending and temperature of the hotspot at breakage.

Instrument	Angle of breakage	Torque at breakage	Time to breakage	Temperature of hotspot at breakage
	[deg]	[N cm]	[s]	[^{o}C]
EDM 40.04	376.32 ± 20.25^{a}	1.080 ± 0.052^{a}	31.365 ± 0.442^{a}	32.7 ± 1.3^{a}
CM 40.04	241.44 ± 12.15^{b}	1.364 ± 0.29^{b}	20.127 ± 0.123^{b}	31.4 ± 0.2^{b}
	Different superscript letters in the same column show statistically significant difference ($P > 0.05$)			
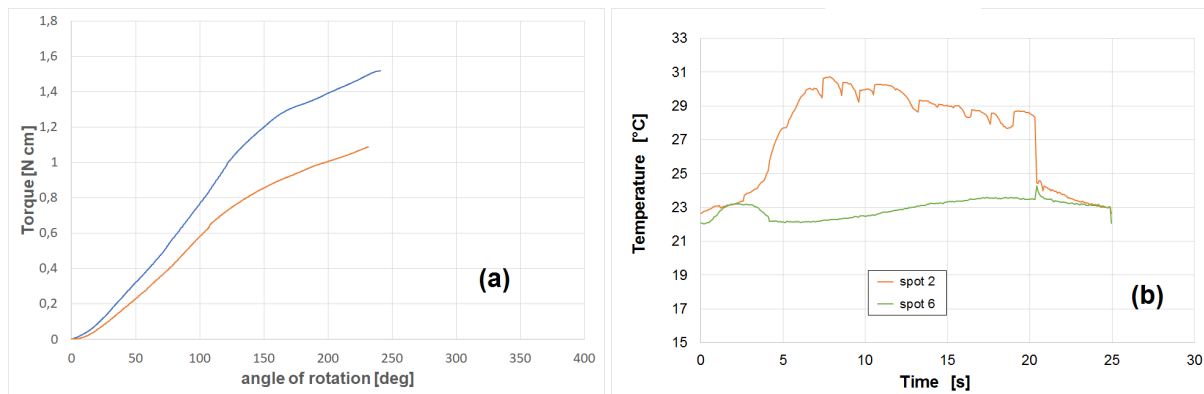
Figure 4: (a) Mechanical and (b) Thermal diagrams of CM 40.04 endodontic instrument.
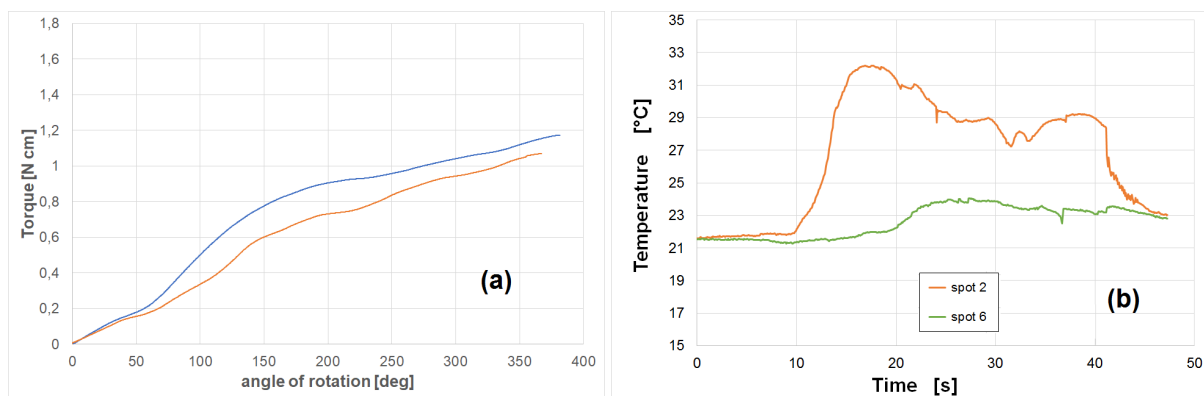
Figure 5: (a) Mechanical and (b) Thermal diagrams of EDM 40.04 endodontic instrument.

Austenite phase el. modulus E1	Transitory phase el. modulus E2	Martensite phase el. modulus E3
[GPa]	[MPa]	[GPa]
35,7	860	35,7
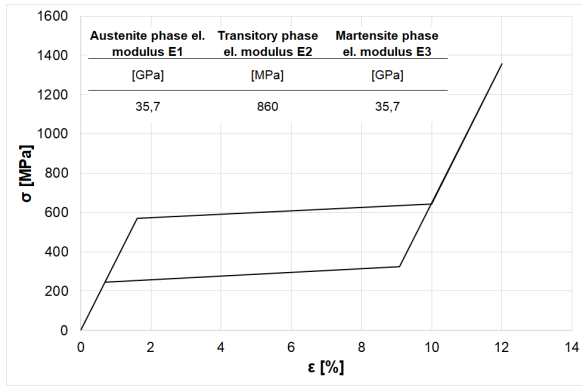
Figure 6: NiTi alloy behavior.
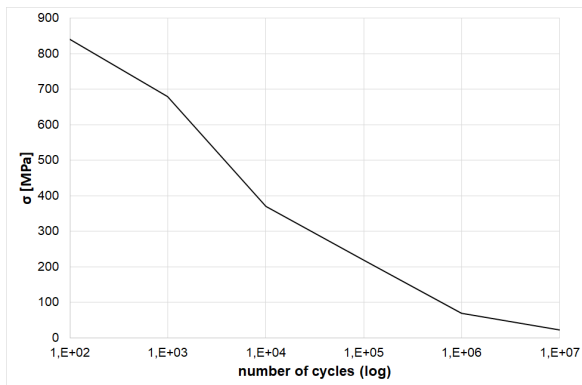
Figure 7: NiTi alloy S-N curve.

3. Numerical Simulation

The elastoplastic material behavior was synthetized in Solidworks Simulation environment with a non-linear elastic material model. A non-linear elastic constitutive curve was computed to ensure the simulation of the superelastic characteristics of the material behavior (Fig. 6). This curve was computed starting from previous models available in the scientific literature [13, 14, 15, 16], while the fatigue behavior was modelled with the S-N curve [17, 18, 19] shown in Fig. 7.

Von Mises maximum stress criteria were adopted to identify the material failure under bending and torsional stress. The finite-elements method simulating torsional and bending failure consists of a nonlinear static analysis for both the above-mentioned models and types of excitation. The nonlinear analysis methodology allowed to include the time dependence of large strain on the model in according to a well-defined material behavior and an opportune set of boundary conditions.

Therefore, force-controlled multi-step and quasi-static computing was adopted for both the two types of excitation. The geometrical shape of both rotary file types was replicated in CAD environment starting from micro-tomographic detections on relative commercial products.

Meshes of the CAD models were made according to the Voronoi-Delaunay algorithm with 16 Jacobian points per element.

4. FEA on cyclic fatigue tested samples

The mesh of CM 40.04 counted 21,582 nodes and 12,398 tetrahedral elements (elements size of 0.12±0.005 mm), while the EDM 40.04 mesh consisted of 23,357 nodes and 13,805 tetrahedral elements (elements size of 0.15± 0.01 mm). The maximum Jacobian ratio was 5.86 for CM 40.04 and 7.64 for EDM 40.04. The maximum aspect ratio returned was 12.206 for CM 40.04 and 9.504 for EDM 40.04. Boundary conditions were applied under the prevision of a 5 mm curvature radius [7]. In fact, a remote displacement through rigid beams was imposed to the normal cross-section of the file at a distance of 2 mm from the file tip, while a fixed constraint was set to the corresponding normal cross- section of the file located at a distance equal to 8.24 mm from the former one. The imposed displacements consisted of the angle of bending ($\alpha = 60^o$) and orthogonal components of the cross- section translation in the plane (0.91 mm along the file axis, 2.5 mm normal to the file axis), respectively [7]. The resultant will be a circle arc corresponding to an angle equals to 60° and radius equals to 5 mm. With notation x as the file axis, calculations were performed in four different directions of bending, along the coordinated planes x,y and x,z in order to discretize the rotating bending excitation. Figures 8a,b show Von Mises stress distribution at 60 degrees bending on CM 40.04 and EDM 40.04, respectively. Responses from the bending simulations reported agreement with the experimental results. Simulated bending of the two models indicated that the simple imposed flexion in the above-mentioned conditions did not produce a complete martensite phase transformation.

A fatigue numerical simulation was performed in order to verify the damage state of the material in both CM 40.04 and EDM 40.04 files. An event-dependent analysis was implemented setting up a four-event cyclic calculation starting from the bending analysis previously described. The fatigue analysis leaded back to the meshes relative to the bending analysis. Moreover,
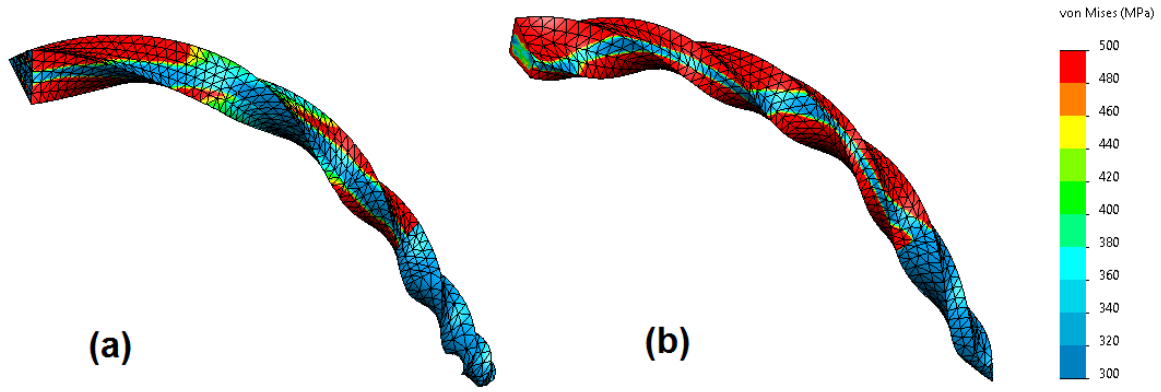
Figure 8: Von Mises stress distribution at 60 degrees bending on (a) CM 40.04 and (b) EDM 40.04.
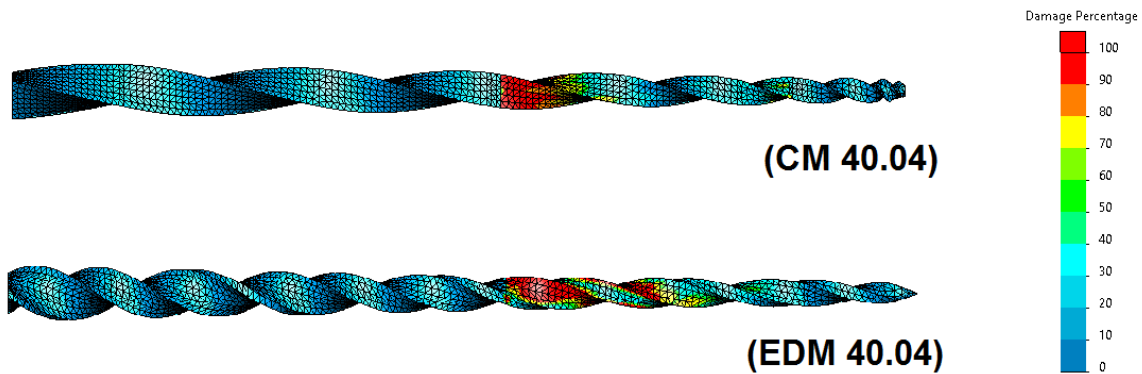
Figure 9: CM 40.04 and EDM 40.04 damage percentage.

each event was set as an impulsive load (R = 0) and imposed on the mesh model. The number of cycles reported agreements with the experimental tests. In fact, the damage diagrams for both the models indicated a nodal distribution at 100% of material damage at 1,490 cycles for CM 40.04 and 1,840 cycles for EDM 40.04, respectively (Fig. 9).

5. FEA on cyclic fatigue tested samples

The mesh of CM 40.04 counted 42,897 nodes and 27,163 tetrahedral elements (element size of 0.12 ± 0.005 mm), while that of EDM 40.04 consisted of 42,336 nodes and 26,809 tetrahedral elements (element size of 0.15 ± 0.01 mm). The maximum Jacobian ratio was 4.98 for CM 40.04 and 7.21 for EDM 40.04, respectively. The maximum aspect ratio returned was 10.306 for CM 40.04

and 8.841 for EDM 40.04, as a confirmation of the good quality of the models. Boundary conditions were applied with a fixed constraint on the cutter surfaces relative to the grip (5 mm from the file tip) and a hinge joint constraint to the file stem. Remote time-dependent displacements through rigid beams were applied to the last cross-section of the stem, at the drive connection, in order to simulate the torsion deformation. These displacements were consisted in a revolution of the ultimate stem cross- section relative to the rotating driver around the file axis. Deformations were progressively applied with a linear time dependence to ensure a rotational velocity simulation of 2 rpm for both the models. Results confirmed compliance with the model of the material constitutive curve. Simulated time-to- failure durations returned strain values of 22.11 s for CM 40.04 and 30.55 s for EDM 40.04, relative to failure angles equal to 265.32^{o} for CM 40.04 and 366.624^{o} EDM 40.04, respectively. It has to be noted
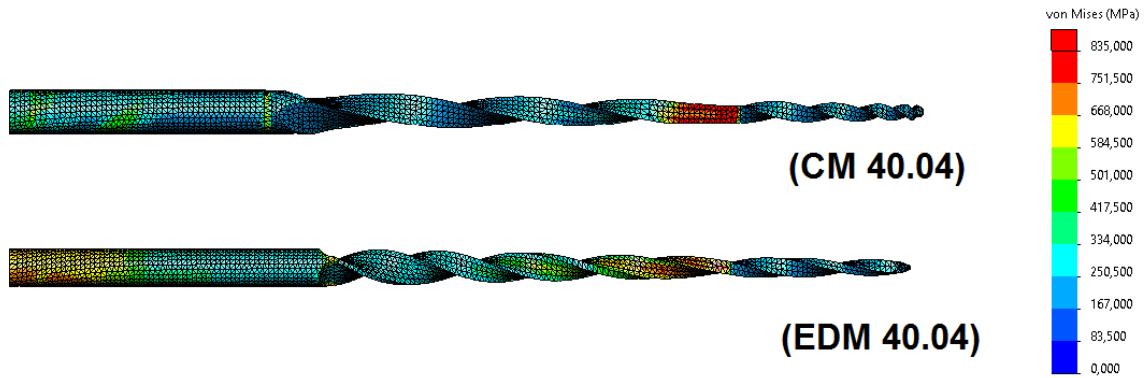
Figure 10: CM 40.04 and EDM 40.04 torsional stress.
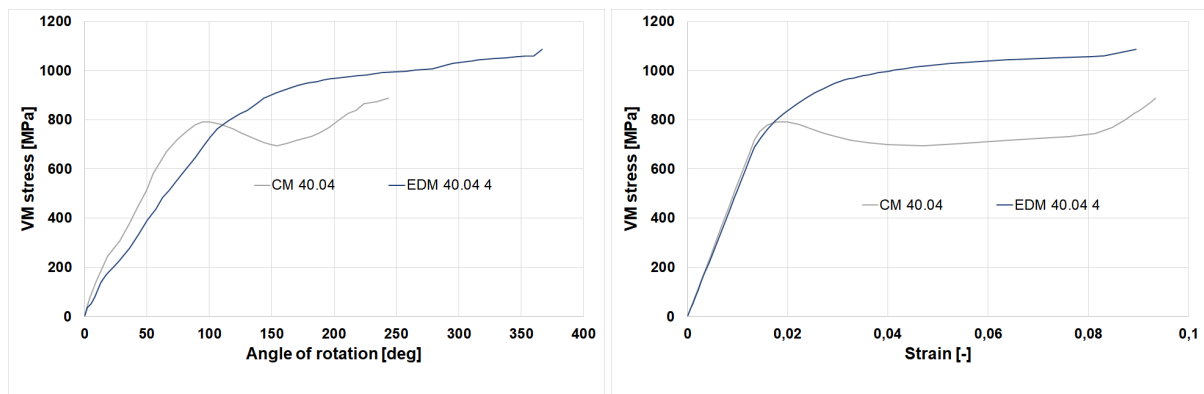
Figure 11: Simulated phase transformation for (a) rotation and (b) strain of the most stressed element.

how the breakage location was well predictable and recognized on both the models (Fig. 10). Analysis returned that the most stressed zone was computed at 0.93 mm from the grip for CM 40.04 and at 0.29 mm from the grip for EDM 40.04. Moreover, stress-strain curves relative to the most stressed element were extrapolated from the FEA. Figures 11a,b show the simulated phase transformation for rotation and strain of the most stressed element, respectively. It is clear that the failure occurs in the martensite phase for both the models.

6. Results and Conclusion

An accurate numerical simulation and experimental tests on two different rotary endodontic files were performed in order to analyse both the cyclic fatigue and torsional behaviour. Simultaneous thermographic investigation was a helpful element of validation of results.

References

[1] Y. Jia, Y. Gao, Metallurgical characterization of m-wire nickel-titanium shape memory alloy used for endodontic rotary instruments during low-cycle fatigue, Journal of Endodontics 38 (2012).

[2] N. J. Bechle, S. Kyriakides, Evolution of phase transformation fronts and associated thermal effects in a niti tube under a biaxial stress state, Extreme Mechanics Letters (2016).

[3] B. Martín, G. Zelada, P. Varela, J. G. Bahillo, F. Magán, S. Ahn, C. Rodríguez, Factors influencing the fracture of nickel-titanium rotary instruments, International Endodontic Journal 36 (2003).

[4] X. Xu, M. Eng, Y. Zheng, D. Eng, Comparative study of torsional and bending properties for six models of nickel-titanium root canal instruments with different cross-sections, Journal of Endodontics 32 (2006) 372–375.

[5] G. La Rosa, F. Lo Savio, E. Pedullà, E. Rapisarda,

A new torquemeter to measure the influence of heat-treatment on torsional resistance of niti endodontic instruments, Engineering Failure Analysis 82 (2017) 446–457.

[6] F. Lo Savio, G. La Rosa, M. Bonfanti, D. Alizzio, E. Rapisarda, E. Pedullà, Novel cyclic fatigue testing machine for endodontic files, Experimental Techniques 44 (2020) 649–665.

[7] E. Pedullà, F. Lo Savio, S. Boninelli, G. Plotino, N. M. Grande, G. La Rosa, E. Rapisarda, Torsional and cyclic fatigue resistance of a new nickel-titanium instrument manufactured by electrical discharge machining, Journal of endodontics 42 (2016) 156–159.

[8] G. Plotino, N. Grande, M. Melo, M. Bahia, L. Testarelli, G. Gambarini, Cyclic fatigue of niti rotary instruments in a simulated apical abrupt curvature, International Endodontic Journal 43 (2010) 226–230.

[9] A. M. Elnaghy, S. E. Elsaka, Torsion and bending properties of oneshape and waveone instruments, Journal of endodontics 41 (2015) 544–547.

[10] H. Kim, H. Kim, C. Lee, B. Kim, J. Park, A. Versluis, Mechanical response of nickel–titanium instruments with different cross-sectional designs during shaping of simulated curved canals, International Endodontic Journal 42 (2009) 593–602.

[11] F. Lo Savio, E. Pedullà, E. Rapisarda, G. La Rosa, Influence of heat-treatment on torsional resistance to fracture of nickel-titanium endodontic instruments, Procedia Structural Integrity 2 (2016) 1311–1318.

[12] F. Lo Savio, E. Pedullà, E. Rapisarda, G. La Rosa, Influence of heat-treatment on torsional resistance to fracture of nickel-titanium endodontic instruments, Procedia Structural Integrity 2 (2016) 1311–1318.

[13] E. Berutti, G. Chiandussi, I. Gaviglio, A. Ibba, Comparative analysis of torsional and bending stresses in two mathematical models of nickel-titanium rotary instruments: Protaper versus profile, Journal of Endodontics 29 (2003) 15–19.

[14] V. Chevalier, L. Pino, R. A. Chirani, S. Calloch, S. A. Chirani, Experimental validation of numerical simulations of a new-generation niti endodontic file under bending, Journal of Materials Engineering and Performance 27 (2018) 5856–5864.

[15] G. Carpegna, M. Alovisi, D. S. Paolino, A. Marchetti, U. Gibello, N. Scotti, D. Pasqualini, A. Scattina, G. Chiandussi, E. Berutti, Evaluation of pressure distribution against root canal walls of niti rotary instruments by finite element

[16] N. Bonessio, E. Pereira, G. Lomiento, A. Arias, M. Bahia, V. T. L. Buono, O. A. Peters, Validated finite element analyses of waveone endodontic instruments: a comparison between m-wire and niti alloys, International Endodontic Journal 48 (2015) 441–450.

[17] P. Ramu, S. Arul, Estimating probabilistic fatigue of nitinol with scarce samples, International Journal of Fatigue 85 (2016) 31–39.

[18] M. I. El-Anwar, A. O. Mandorah, S. A. Yousief, T. A. Soliman, T. M. A. El-Wahab, A finite element study on the mechanical behavior of reciprocating endodontic files, Brazilian Journal of Oral Sciences 14 (2015) 52–59.

[19] G. Cheung, E. Zhang, Y. Zheng, A numerical method for predicting the bending fatigue life of niti and stainless steel root canal instruments, International endodontic journal 44 (2011) 357–361.

[20] G. La Rosa, C. Clienti, A. M. C. Garrano, F. Lo Savio, Low-cycle fatigue hysteresis by thermographic and digital image correlation methodologies: a first approach, Procedia Structural Integrity 13 (2018) 1583–1588.

[21] R. Montanini, A. Quattrocchi, S. A. Piccolo, A. Amato, S. Trocino, S. C. Zignani, M. L. Faro, G. Squadrito, Real-time thermal imaging of solid oxide fuel cell cathode activity in working condition, Applied optics 55 (2016) 7142–7148.

[22] A. Risitano, G. La Rosa, A. Geraci, E. Guglielmino, The choice of thermal analysis to evaluate the monoaxial fatigue strength on materials and mechanical components, Proceedings of the Institution of Mechanical Engineers, Part C: Journal of Mechanical Engineering Science 229 (2015) 1315–1326.